Geophysical Research Letters

RESEARCH LETTER
10.1029/2023GL107833

Strong Aerosol Absorption and Its Radiative Effects in Lhasa on the Tibetan Plateau

Shuo Wang[1], Weixiong Zhao[1,2], Qianqian Liu[1,2], Jiacheng Zhou[1], Suzanne Crumeyrolle[3], Xuezhe Xu[1], Chong Zhang[4], Chunxiang Ye[4], Yu Zheng[5], Huizheng Che[5], and Weijun Zhang[1,2]

[1]Laboratory of Atmospheric Physico-Chemistry, Anhui Institute of Optics and Fine Mechanics, HFIPS, Chinese Academy of Sciences, Hefei, China, [2]School of Environmental Science and Optoelectronic Technology, University of Science and Technology of China, Hefei, China, [3]LOA - Laboratoire d'Optique Atmosphérique, CNRS, UMR 8518, Université Lille, Lille, France, [4]State Key Joint Laboratory for Environmental Simulation and Pollution Control, College of Environmental Sciences and Engineering, Peking University, Beijing, China, [5]State Key Laboratory of Severe Weather & Key Laboratory of Atmospheric Chemistry, Institute of Atmospheric Composition and Environmental Meteorology, Chinese Academy of Meteorological Sciences, China Meteorological Administration, Beijing, China

Abstract Knowledge of aerosol radiative effects in the Tibetan Plateau (TP) is limited due to the lack of reliable aerosol optical properties, especially the single scattering albedo (SSA). We firstly reported in situ measurement of SSA in Lhasa using a cavity enhanced albedometer (CEA) at $\lambda = 532$ nm from 22nd May to 11th June 2021. Unexpected strong aerosol absorbing ability was observed with an average SSA of 0.69. Based on spectral absorptions measured by Aethalometer (AE33), black carbon (BC) was found to be the dominated absorbing species, accounting for about 83% at $\lambda = 370$ nm, followed by primary and secondary brown carbon (BrC_{pri} and BrC_{sec}). The average direct aerosol radiative forcing at the top of atmosphere ($DARF^{TOA}$) was 2.83 W/m^2, indicating aerosol warming effect on the Earth-atmosphere system. Even though aerosol loading is low, aerosol heating effect plays a significant role on TP warming due to strong absorbing ability.

Plain Language Summary The Tibetan Plateau (TP) has experienced rapid warming over the past decades, but the key factors affecting TP climate change haven't yet been clearly understood. Aerosol single scattering albedo (SSA) is a key optical parameter determining aerosol warming or cooling effect; however, reliable SSA measurement is scarce in TP. This study firstly reported in situ measurement of SSA in Lhasa and explored the direct radiative effect of aerosol on TP warming. Strong aerosol absorption, mainly contributed by black carbon (BC), was observed with an average SSA value of 0.69 in this city. Besides Lhasa, other sites over TP were also reported with low SSA (≤0.77) from surface measurement. The strong aerosol absorption could cause heating effect on the Earth-atmosphere system. To relieve TP warming, reasonable pollutant emission control strategies should be taken urgently to weaken aerosol absorbing ability.

Key Points:

- Unexpected low aerosol single scattering albedo was observed in Lhasa via in situ measurement of multiple optical parameters simultaneously
- Black carbon was the dominant contributor (~83%) to aerosol absorption at 370 nm, followed by primary and secondary brown carbon
- The strong absorption in Lhasa exerted positive direct aerosol radiative forcing (warming effect) at the top of atmosphere

Supporting Information:

Supporting Information may be found in the online version of this article.

Correspondence to:

W. Zhao and W. Zhang,
wxzhao@aiofm.ac.cn;
wjzhang@aiofm.ac.cn

Citation:

Wang, S., Zhao, W., Liu, Q., Zhou, J., Crumeyrolle, S., Xu, X., et al. (2024). Strong aerosol absorption and its radiative effects in Lhasa on the Tibetan Plateau. *Geophysical Research Letters*, *51*, e2023GL107833. https://doi.org/10.1029/2023GL107833

Received 13 DEC 2023
Accepted 12 MAR 2024

1. Introduction

The Tibetan Plateau (TP) is the third pole with high altitude and strong radiation, located in the west of China. Over the past 50 years, there has been a growing concern that the warming rate over TP is twice more than the global average value (Kang et al., 2016; Mu et al., 2020; You et al., 2021). TP warming impacts not only local ecosystem but also regional or global atmospheric and climate changes (Huang et al., 2023; Wang et al., 2008). Moreover, there are large spatial heterogeneities in the air temperature increase in TP (Mu et al., 2020), adding complexity to figure out the driving mechanisms. Previous studies attributed accelerated TP warming to cloud-radiation feedback (Duan & Xiao, 2015), stratospheric ozone depletion (Guo & Wang, 2012), CO_2 (Chen et al., 2002) or water vapor (Rangwala et al., 2009) increasing concentrations. However, the reasons of TP warming have not reached an agreement by now.

Aerosol has significant impacts on radiation balance of the Earth-atmosphere system by scattering and absorption of solar radiation (Chylek & Wong, 1995; Gui et al., 2022; Li et al., 2022; Ramanathan et al., 2005). The aerosol scattering or absorbing ability is represented by single scattering albedo (SSA). Stronger aerosol scattering ability (with larger SSA) can enhance reflected solar radiation from the Earth causing cooling effect, while aerosol absorbing (with lower SSA) leads to positive net radiation and contributes to warming effect. Among 31 sites connected to the Global Atmosphere Watch (GAW) network, the SSA mean values based on in situ measurement

ranged from 0.8 to 1, with only six sites lower than 0.9 (Laj et al., 2020). SSA is the most sensitive factor to aerosol radiative forcing calculation compared with other optical parameters (Loeb & Su, 2010; Lu et al., 2022; McComiskey et al., 2008). Inorganic aerosols, like nitrate and sulfate, are treated as pure scattering aerosol. The absorbing aerosols include black carbon (BC), brown carbon (BrC) and dust. BC is the primary pollutant from incomplete combustion processes (Bond et al., 2013), while BrC can be produced from primary emission (BrC_{pri}) (Saleh et al., 2014) and secondary chemical reactions (BrC_{sec}) (Lambe et al., 2013). Deriving absorptions by different aerosols is helpful to identify the potential impactors, which could provide scientific basis for policy makers to balance different aerosol emissions.

Remote sensing observations showed that aerosol optical depth (AOD) in TP could be 10 times lower compared with sites in eastern China (de Leeuw et al., 2018; Li, Li, et al., 2020; Li, Xiao, et al., 2020; Lu et al., 2022). Previous studies evaluated that aerosol over TP had weak impact on radiative forcing based on ground based remote sensing observation, as it was less efficient to warm the atmosphere due to the low aerosol loading (Li, Li, et al., 2020; Li, Xiao, et al., 2020). However, aerosol radiative effects over TP still have large uncertainties because of inaccurate knowledge of aerosol optical properties, especially SSA. For example, quality-assured SSA retrieved from sun photometer is only available for AOD larger than 0.4 at 440 nm (Dubovik et al., 2000; Dubovik & King, 2000; Holben et al., 2006), while AOD is usually lower than 0.2 over TP (Zhu et al., 2019). Moreover, SSA retrieved from satellite observations are missing over TP (Ramachandran et al., 2020), and the retrieved SSA values depend highly on the retrieval algorithms (Devi & Satheesh, 2022). The lack of reliable SSA observed or retrieved over TP leads to large uncertainties to assess aerosol radiative forcing in this region.

Lhasa is the capital city of Tibet province, with the largest population (around 460,000 inhabitants). Zhu et al. (2019) reported that the yearly average AOD at 440 nm was lower than 0.2 in Lhasa. Apart from the low aerosol content, aerosol composition in Lhasa exhibits distinctive characteristics. Based on in situ measurements, Zhao et al. (2022) found lower concentration of secondary inorganic aerosols (by a factor of 2–5 times) in comparison to similar cities in eastern China (Huang et al., 2014; Sun et al., 2015), with nitrate and sulfate fractions of 5.4% and 3.4%, respectively. Zhu et al. (2017) revealed that Lhasa had low absorption Ångström exponent (AAE = 1.04) over the whole measured spectral range (370–950 nm), with large contribution of black carbon (>90%) and low contribution of brown carbon and dust. By now, the reliable SSA hasn't been reported in Lhasa, and absorption by BrC_{sec} is still unknown.

In this work, in situ measurements were performed in Lhasa to obtain multiple aerosol optical parameters combining the cavity enhanced albedometer (CEA) and Aethalometer (AE33), including aerosol extinction, scattering, absorption coefficients and SSA at λ = 532 nm, as well as absorption coefficients at multiple wavelengths. The absorption contributions by different aerosols were distinguished to further identify the main compounds impacting on aerosol absorption in this city. Clear-sky direct aerosol radiative forcing (DARF) was then evaluated based on measured aerosol optical properties by using the Santa Barbara Discrete Ordinate Atmospheric Radiative Transfer (SBDART) model. Positive aerosol radiative forcing at the top of atmosphere was revealed due to strong absorption during the campaign, indicating that aerosol might play a significant role on TP warming.

2. Methods

2.1. Observation Site

Lhasa is located in the southern TP and characterized with its river valley terrain (Figure S1 in Supporting Information S1), surrounded by high mountains (over 5,500 m a.s.l), which prevents aerosol pollutants from dispersion. Aerosols in Lhasa are mainly issued from local anthropogenic activities, like traffic emissions, religious activities, coal combustion (Zhao et al., 2022), as well as long-range transport from South Asia (Chen et al., 2022). The field campaign was conducted in the Institute of Tibetan Plateau Research (29.63°N, 91.02°E, 3,640 m a.s.l.) from 22nd May to 11th June 2021. The observation site is located in the western part of urban Lhasa, and it is closed to Jinzhu Road, which is a major road in Lhasa with heavy traffic.

2.2. Aerosol Optical Properties and Meteorological Factors Measurements

CEA measures aerosol extinction and scattering coefficients at λ = 532 nm in the same sample volume simultaneously (Xu et al., 2018; Zhao et al., 2014; Zhou et al., 2020). Aerosol absorption coefficient and SSA can be

obtained from the difference and ratio of both measurements. The uncertainties of extinction, scattering and absorption coefficients and SSA are 3.3%, 3%, 4.5%, and 5.5%, respectively (Xu et al., 2018). AE33 measures aerosol absorptions at seven wavelengths (λ = 370, 470, 520, 590, 660, 880, and 950 nm) by using filter-based method (Drinovec et al., 2015). The AAE is expressed as the absorption dependence on wavelength, and it can be obtained with absorption coefficients at two wavelengths (λ and λ_0) as shown in Equation 1. Using spectral variation of absorption coefficients, AAE was calculated as the slope of least-square fit of the logarithm of Abs(λ) versus the logarithm of seven wavelengths in this study (Helin et al., 2021). During the campaign, ambient aerosol particles passed through a $PM_{2.5}$ cyclone inlet and a Nafion dryer upstream the CEA and AE33 to measure dry $PM_{2.5}$ optical properties. The flowrates were set at 1.3 and 3 L min^{-1} for CEA and AE33, respectively. To get the absorption coefficient correction factor measured by AE33 due to multiple scattering, aerosol absorption at λ = 532 nm determined by CEA was used as the reference (Li, Li, et al., 2020; Li, Xiao, et al., 2020). Since multiple scattering correction factor is wavelength-independent (Saleh et al., 2014; Zhao et al., 2020), the correction factor (2.62 for this study, Figure S2 in Supporting Information S1) could be also used for other wavelengths to obtain reasonable aerosol absorptions. The Cimel sun photometer (CE318) installed in Lhasa (29.6°N, 91.2°E) was used to obtain AOD at λ = 380, 440, 500, 670, 870, and 1,020 nm during the daytime.

$$AAE_{\lambda-\lambda_0} = -\frac{\ln(Abs(\lambda)/Abs(\lambda_0))}{\ln(\lambda/\lambda_0)} \quad (1)$$

Apart from aerosol optical properties, meteorological factors were measured during the campaign, including temperature and relative humility (RH) measured by meteorological sensor (HMP155A, Vaisala), wind speed and direction measured by a sensor (010C-1/020C-1, Metone), as well as upward and downward shortwave radiation observed by radiometer (300–2,800 nm for shortwave, CNR4, Kipp & Zonen). The date and time reported in this study are using China standard time (CST: UTC + 8 h).

2.3. Identification of BC, BrC_{pri}, and BrC_{sec}

Previous study revealed Lhasa was rarely impacted by dust from May to September, as the observed PM_{10} concentration and crustal elements (Na, Mg, Al, Ca, etc.) were significantly lower during this period (Cong et al., 2011). Ignoring the impact by dust, BC and BrC are treated as the only absorbers within the $PM_{2.5}$ fraction during the campaign. Primary BC and BrC are mainly emitted from combustion processes. The minimum R-squared (MRS) method was used to differentiate BrC_{sec} from primary BC and BrC (Wang et al., 2019; Wu et al., 2018; Zhu et al., 2021). First, the absorption coefficient by primary aerosols is estimated using the following equation:

$$Abs_{pri}(\lambda) = (Abs(\lambda)/BC)_{pri} \times [BC] \quad (2)$$

Where [BC] is the mass concentration of BC, and $(Abs(\lambda)/BC)_{pri}$ can be assumed to a constant value for a specific season at specific region (ranging from 0 to 100 with step of 0.01). BrC_{sec} absorption is then calculated by the total absorption subtracting absorptions by primary BC and BrC (Equation 3) assuming different values of $(Abs(\lambda)/BC)_{pri}$. The optimal $(Abs(\lambda)/BC)_{pri}$ is determined when absorptions of calculated BrC_{sec} and [BC] have minimum correlation coefficient (R^2).

$$Abs_{BrC,sec}(\lambda) = Abs(\lambda) - (Abs(\lambda)/BC)_{pri} \times [BC] \quad (3)$$

Considering that the AAE of BC (AAE_{BC}) differs with BC size distribution (Li, Liu, et al., 2016; Li, Chen, et al., 2016; Wang et al., 2016), assuming AAE_{BC} of 1 may bring larger uncertainties. In this study, AAE_{BC} was assumed to be equal to AAE calculated at λ = 880 and 950 nm ($AAE_{880\text{-}950}$, Equation 4). Because BC is usually treated as the only absorbing aerosol at both wavelengths and previous experiment proved that $AAE_{880\text{-}950}$ values were almost the same before and after removing other absorbing aerosols and the coating (Zhang et al., 2019). Therefore, absorption of BrC_{pri} can be derived by subtracting BC absorption with previously calculated absorptions of primary aerosol (Equation 5).

$$Abs_{BC}(\lambda) = Abs(880) \times (\lambda/880)^{-AAE_{880-950}} \quad (4)$$

$$\mathrm{Abs}_{\mathrm{BrC,pri}}(\lambda) = \mathrm{Abs}_{\mathrm{pri}}(\lambda) - \mathrm{Abs}_{\mathrm{BC}}(\lambda) \quad (5)$$

2.4. Calculation of Aerosol Radiative Effects

The net radiation flux is the difference between downward ($F^{\downarrow}$) and upward ($F^{\uparrow}$) radiation flux (Equation 6). Direct aerosol radiative forcing at the top of atmosphere ($\mathrm{DARF}^{\mathrm{TOA}}$) or the bottom ($\mathrm{DARF}^{\mathrm{BOT}}$) is defined as the net change in radiative flux caused by aerosols in the atmosphere (Equations 7 and 8).

$$F_{\mathrm{net}} = F^{\downarrow} - F^{\uparrow} \quad (6)$$

$$\mathrm{DARF}^{\mathrm{TOA}} = {F_{\mathrm{net,aerosol}}}^{\mathrm{TOA}} - {F_{\mathrm{net,noaerosol}}}^{\mathrm{TOA}} \quad (7)$$

$$\mathrm{DARF}^{\mathrm{BOT}} = {F_{\mathrm{net,aerosol}}}^{\mathrm{BOT}} - {F_{\mathrm{net,noaerosol}}}^{\mathrm{BOT}} \quad (8)$$

$$\mathrm{DARF}^{\mathrm{ATM}} = \mathrm{DARF}^{\mathrm{TOA}} - \mathrm{DARF}^{\mathrm{BOT}} \quad (9)$$

The difference between $\mathrm{DARF}^{\mathrm{TOA}}$ and $\mathrm{DARF}^{\mathrm{BOT}}$ is calculated as the direct aerosol radiative forcing in the atmosphere ($\mathrm{DARF}^{\mathrm{ATM}}$). Radiation flux was calculated with SBDART model (Ricchiazzi et al., 1998), which was widely used to evaluate aerosol radiative effects using column integrated (Lu et al., 2022) or vertically resolved optical properties (Su et al., 2020) or a combination of those with surface measurements (Kuang et al., 2015). The input optical parameters to SBDART included AOD and Extinction Ångstrom Exponent (EAE) from CE318, SSA measured by CEA, and surface albedo calculated as the ratio of measured upward to downward shortwave radiation. Previous study (Lu et al., 2022) reported that DARF was less sensitive to asymmetric factor compared with AOD and SSA (Loeb & Su, 2010). This study used the average asymmetric factor of 0.71 reported at Namco site, which is close to Lhasa (Lu et al., 2022).

3. Results

3.1. Variation of Meteorological Factors and Aerosol Optical Properties

Variations of shortwave radiation and meteorological factors are given in Figures 1a–1c. The peak value of downward shortwave radiation during daytime was around 1400 W/m^2, which is twice higher than sites in Yangtze River Delta (YRD) of China (Duan et al., 2022). The average temperature was 17.6 ± 4.2°C during the campaign. RH had an average value of 40.1 ± 17.5% and was usually below 50% (taking about 79%), so aerosol hygroscopic growth effect can be ignored for most cases and the measured dry aerosol optical properties can represent the result in the real atmosphere (Tao et al., 2014; Yan et al., 2009). Episodically, RH could reach values larger than 80%, but it only occurred during nighttime. Wind speed was usually lower than 3 m/s with an average value of 1.1 ± 0.8 m/s, and the most frequent (46%) wind direction was southwest with high wind speed (around 2 m/s).

Aerosol optical properties variations during the campaign are shown in Figures 1d and 1e. It could be found that aerosol loading was generally low in Lhasa with average extinction, scattering and absorption coefficients of 13.6 ± 10.7, 9.3 ± 7.2 and 4.3 ± 4.0 Mm^{-1}, respectively. Extinction coefficient was usually lower than 20 Mm^{-1} (for about 86% of the period). There was no obvious regional pollution episode during the campaign except for some peaks (extinction coefficient peaked up to 60 Mm^{-1}) caused by local emission starting from 21:00 and lasting for 1–2 hr (Figure S3 in Supporting Information S1). The larger values of aerosol extinction coefficients correspond to the lower values of SSA, meaning large influence of local emission on SSA. These late emissions might be related to traffic emissions due to heavy trucks circulation forbidden during daytime in Lhasa. Furthermore, AOD at 440 nm was lower than 0.2 during the observation, with an average value of 0.08 ± 0.02. SSA ranged from 0.44 to 0.9 with an average value of 0.69 ± 0.09, which is lower than SSA values highlighted by the GAW network (Laj et al., 2020). The low SSA over Lhasa might be due to extremely low contribution from secondary inorganic aerosols (Zhao et al., 2022). In addition, regional transport from South Asia with absorbing aerosols might contribute to low SSA values. As shown in Figure 1 and Figure S4 in Supporting Information S1, lower SSA was observed with an average value of 0.61 ± 0.07 from 20:00 on 25th to 1:00 on 30th May 2021, and air masses during this period were coming from South Asia passing over regions with dense fire spots due to biomass burning (Liu et al., 2021). During observation period, the average AAE was 1.07 ± 0.08, which is close

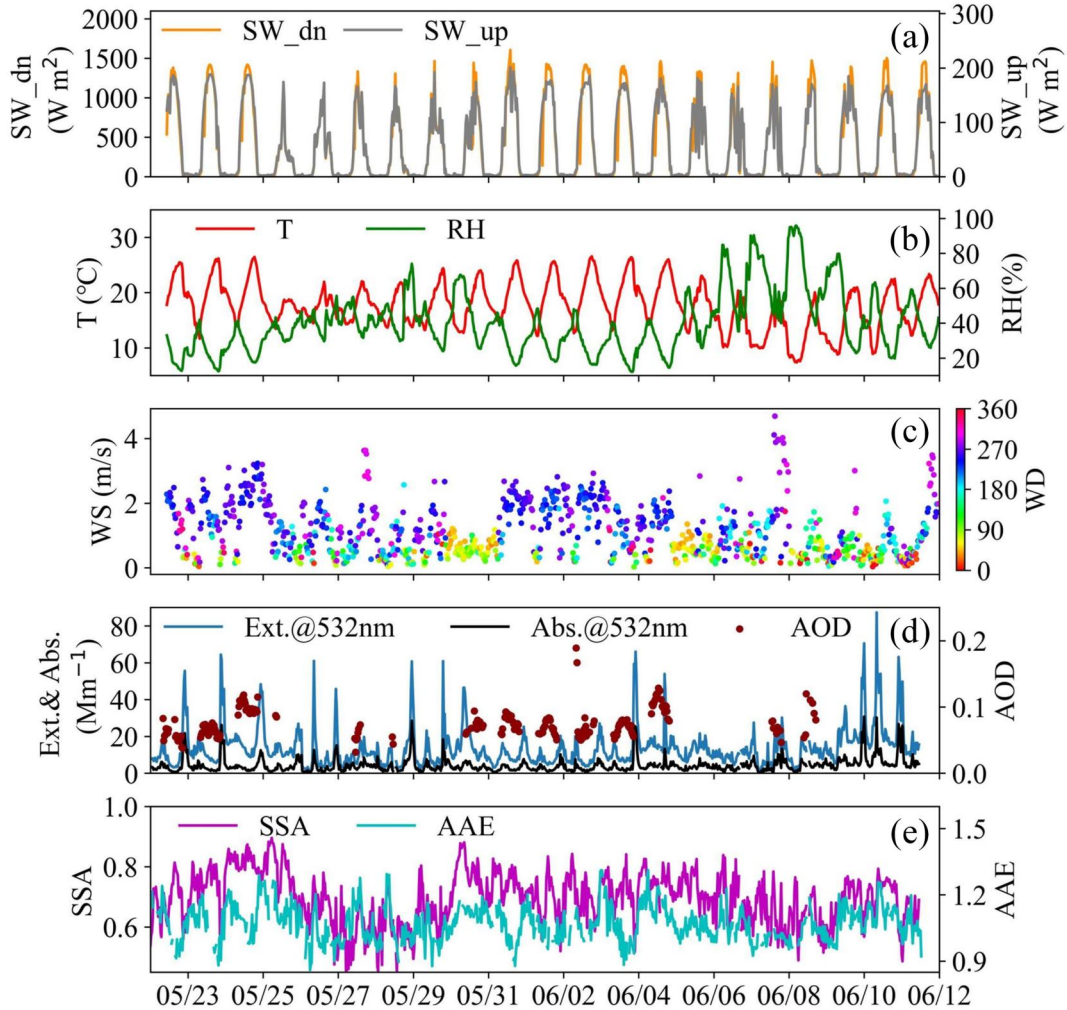

Figure 1. Time series of meteorological factors (downward and upward shortwave radiation: SW_dn and SW_up; temperature: T; relative humility: RH; wind speed and direction: WS and WD) and aerosol optical properties (extinction and absorption coefficients and SSA at 532 nm: Ext. and Abs.; AOD at 440 nm; fitted AAE from 370 to 950 nm) in Lhasa.

to the AAE of aerosol emissions from fossil fuel (Sandradewi et al., 2008). Table 1 is the list of aerosol extinction coefficients and SSA values among sites in TP, eastern China and Europe. Observation sites located in TP are distinguished with lower extinction coefficients and lower SSA values.

3.2. Identification of BC, BrC_{pri}, and BrC_{sec}

In order to explain what causes the low SSA observed in Lhasa, aerosol absorptions of BC, BrC_{pri} and BrC_{sec} were distinguished with MRS and AAE methods. As shown in Figure 2a, BC was the most important absorbing compound with an average absorption coefficient of 5.6 ± 2.5 Mm^{-1} at λ = 370 nm, followed by BrC_{pri} and BrC_{sec} with average absorption coefficients of 0.71 and 0.45 Mm^{-1}, separately. The absorption contributions by BC, BrC_{pri} and BrC_{sec} were 83%, 11% and 6% at 370 nm, respectively. Previous study (Li, Liu, et al., 2016; Li, Chen, et al., 2016) performed measurement over the same site highlighted that $PM_{2.5}$ in Lhasa was mainly impacted by primary emission and less from secondary formation based on the low ratio of OC/EC (1.46). With the increasing wavelength, absorptions from BrC_{pri} and BrC_{sec} declined sharply. At λ = 520 nm, absorption contributions by BC, BrC_{pri} and BrC_{sec} were around 90%, 8% and 2%, respectively.

Absorptions of BC and BrC_{pri} had similar daily variation (Figure 2b), with higher values in the morning and night due to traffic activities. The decreasing of primary aerosols after 8:00 could be explained by the development of planetary boundary layer (PBL), which diluted pollutants near surface. BrC_{sec} peaked in the morning (8:00)

Table 1
Aerosol Extinction Coefficients and SSA Observed at Different Sites

Extinction	SSA	Site	Period	Wavelength	Instrument	Reference
13.6 Mm^{-1}	*0.69*	*Lhasa*	*May-June 2021*	532 nm	*CEA*	*This study*
5.6 Mm^{-1}	*0.73*	*Yadong*	*June-August 2021*	550 nm	*Neph.[a] & AE33*	*Tian et al.* (2023)
6.0 Mm^{-1}	*0.77*	*Qomolangma*	*May-June 2022*	550 nm	*Neph.[a] & AE33*	*Tian et al.* (2023)
5.2 Mm^{-1}	*0.73*	*Shiquanhe*	*July-August 2019*	870 nm	*PAX[b]*	*Zhang et al.* (2021)
201 Mm^{-1}	0.80	Huairou	November 2014–Janarary 2015	470 nm	CEA	Xu et al. (2016)
353 Mm^{-1}	0.89	Shouxian	December 2016	532 nm	CEA	Wang et al. (2021)
336 Mm^{-1}	0.85	Beijing	February 2015	630 nm	CAPS[c]	Han et al. (2017)
191 Mm^{-1}	0.82	Guangzhou	Janarary 2006	532 nm	Neph.[a] & PAS[d]	Garland et al. (2008)
85.0 Mm^{-1}	0.71	Granada	March 2006–February 2007	550 nm	Neph.[a] & MAAP[e]	Titos et al. (2012)
38.0 Mm^{-1}	0.77	Lille	July 2017–December 2019	525 nm	Neph.[a] & AE33	Velazquez-Garcia et al. (2023)

Note. The rows with italics correspond to sites located in TP. [a]Neph, [b]PAX, [c]CAPS, [d]PAS and [e]MAAP are the abbreviations of integrating Nephelometer, Photoacoustic extinctionmeter, Cavity Attenuated Phase Shift, Photoacoustic Spectrometer and Multi Angle Absorption Photometer, respectively.

indicating the formation of BrC_{sec} due to photochemical reactions after sunrise. After 8:00 BrC_{sec} tended to decrease, which is probably associated to the bleaching of light-absorbing chromophores via oxidative processes and PBL development (Wang et al., 2019). From 8:00 to 17:00, absorptions by BrC_{pri} and BrC_{sec} were comparable with average absorption coefficients at $\lambda = 370$ nm of 1.5 and 1.3 Mm^{-1} separately, indicating the non-negligible role of BrC_{sec} absorption during daytime. The large difference between BrC_{pri} and BrC_{sec} absorptions appeared during the nighttime (after 21:00), which is attributed to the emission of primary aerosols but weak formation of BrC_{sec} without sunlight.

3.3. Implication of Aerosol Radiative Effects

The meteorological conditions in Lhasa were simulated during the observation period using the Weather Research & Forecasting Model (WRF, v4.4), and results showed good performance comparing with surfaced measured meteorological parameters (Figure S5 in Supporting Information S1). The daily averaged RH vertical distribution and PBL height (PBLH) are showed in Figure S6 in Supporting Information S1. It could be found that PBL was

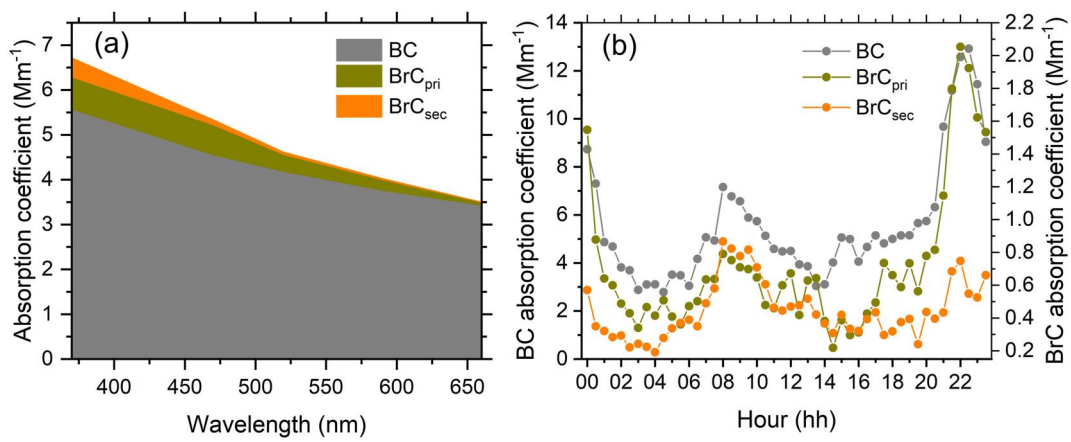

Figure 2. The average spectral absorption coefficients (a) and daily variation of aerosol absorption coefficients (b) by BC, BrC_{pri} and BrC_{sec} at 370 nm.

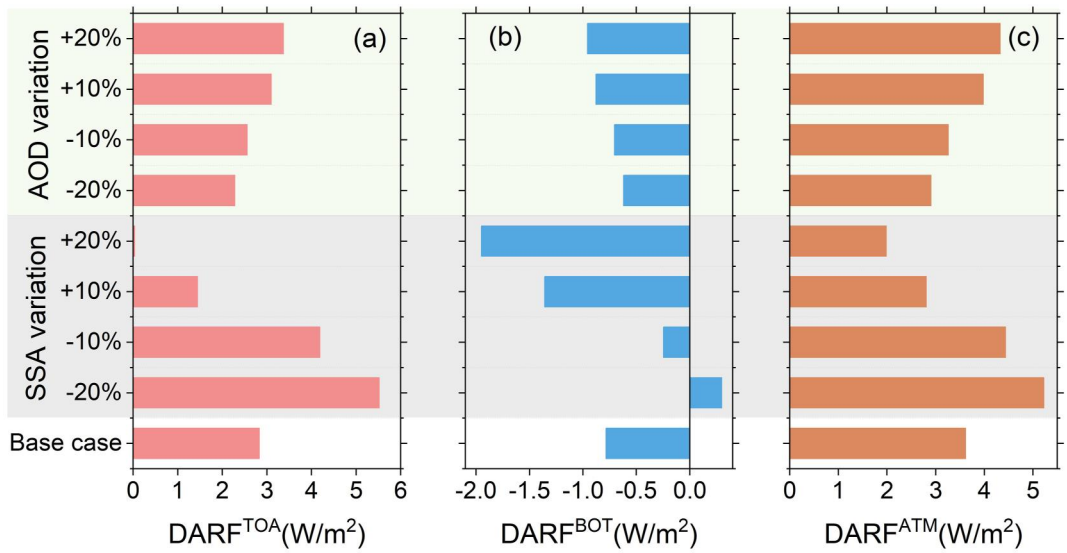

Figure 3. Average $DARF^{TOA}$ (a), $DARF^{BOT}$ (b) and $DARF^{ATM}$ (c) based on aerosol optical properties from 11:00 to 19:00 (base case), and their sensitivities to SSA (gray background) and AOD (green background) with −20%, −10%, 10% and 20% variations.

well developed (PBLH > 1,400 m) from 11:00 to 19:00 in Lhasa, and RH in the PBL was usually lower than 50% except for layers close to the top of PBL. Since organic aerosols are the dominated species over Lhasa with an average contribution of 82.6% (Zhao et al., 2022), which has weaker hygroscopicity compared with inorganic aerosols, such as sulfate and nitrate (Kuang et al., 2020), aerosol hygroscopic growth could be ignored in the PBL over Lhasa during the observation period (Tao et al., 2014; Yan et al., 2009). Assuming that the PBL is well mixed and most aerosol particles are concentrated in the PBL, SSA can be treated as a constant value in the column when PBL is well developed (Li et al., 2017; Ran et al., 2022). To explore DARF sensitivity to aerosol optical properties and minimize the possible SSA uncertainties, $DARF^{TOA}$, $DARF^{BOT}$ and $DARF^{ATM}$ calculated during 11:00–19:00 using SBDART model were set as the base case, and the average AOD and SSA values for this period were 0.06 and 0.70, respectively. The sensitivity experiments were designed via perturbing SSA and AOD values by −10%, −20%, 10% and 20%, respectively.

As shown in Figure 3a, aerosol exerted positive $DARF^{TOA}$ for the base case with an average value of 2.83 W/m^2 from 11:00 to 19:00, which is greater than the global average value of CO_2 effective radiative forcing (2.16 W/m^2) from IPCC Sixth Assessment Report (Masson-Delmotte et al., 2021), indicating strong aerosol heating effect on the Earth-atmosphere system. If SSA decreased by 20% (mean value of 0.56), $DARF^{TOA}$ increased about twice times (5.52 W/m^2). When SSA increased by 10% (SSA = 0.77), $DARF^{TOA}$ decreased to 1.45 W/m^2, but still had warming effect. Only when SSA increased by 20% (SSA = 0.84), aerosol warming effect could be neglected with $DARF^{TOA}$ of 0.04 W/m^2. Compared with SSA, $DARF^{TOA}$ was less sensitive to AOD with only 1.09 W/m^2 difference for AOD varying from −20% to 20%. As given in Table 1, the four sites with surfaced measured low SSA values (SSA ≤0.77) over TP are all locating in the middle and west of TP (Figure S7 in Supporting Information S1), where experienced obvious warming with air temperature increasing rate over 0.06°C per decade from 1901 to 2018 (Mu et al., 2020). This consistency might highlight the non-negligible direct radiative effect of aerosol on TP warming.

The average $DARF^{BOT}$ and $DARF^{ATM}$ were −0.78 and 3.61 W/m^2 for the base case, respectively (Figures 3b and 3c), and their absolute values were extremely low due to the low aerosol content in comparison to results obtained for sites locating in the eastern China (Che et al., 2018; Kuang et al., 2015; Lu et al., 2022; Zheng et al., 2019). For example, Che et al. (2018) reported that the average $DARF^{BOT}$ at different sites ranged from −93 to −79 W/m^2. Similar to $DARF^{TOA}$, $DARF^{BOT}$ and $DARF^{ATM}$ were more sensitive to SSA than AOD. Even though $DARF^{BOT}$ and $DARF^{ATM}$ over Lhasa are very weak compared with sites in eastern China (Che et al., 2018; Kuang et al., 2015; Lu et al., 2022; Zheng et al., 2019), $DARF^{TOA}$ is distinguished with positive value resulting from strong aerosol absorption, implying the vital role of aerosol heating on the Earth-atmosphere system. Considering

that aerosol had increasing trends in most area of TP over the past decades (Rahman et al., 2023; Zhu et al., 2019), that is, the annual AOD trend was about 0.001 years^{-1} from 2007 to 2017 in Lhasa, aerosol warming effect would be strengthened without limiting aerosol emissions. The sensitivity experiments reveal that confining emission fractions of absorbing aerosols, especially BC, is an effective way to reduce DARF^{TOA} and relieve TP warming caused by aerosol.

4. Conclusions

In situ measurement of aerosol optical properties was performed over Lhasa to explore the role of aerosol in TP warming. Unexpected strong absorption was observed in this city, with average SSA of 0.69. This value is significantly smaller than SSA observed over sites in eastern China, and even lower than most of GAW sites in the globe, implying the potential heating effect on the Earth-atmosphere system by aerosol and non-negligible contribution to TP warming. BC, BrC$_{pri}$ and BrC$_{sec}$ contributions to absorption were distinguished combining MRS with AAE method to identify the key compounds influencing the strong absorption. BC was the main absorption contributor, accounting for 83% and 90% at $\lambda = 370$ and 520 nm, respectively. Despite the low aerosol content in Lhasa (average AOD of 0.08 at 440 nm and extinction coefficient of 13.6 Mm^{-1} at 532 nm), aerosol had positive DARF^{TOA} (average value of 2.83 W/m^2 from 11:00 to 19:00) due to its strong absorbing property. As other three sites over TP were also reported with low SSA values ($\leq$0.77) and with obvious warming trend over the past decades (>0.06°C per decade), aerosol might exert a significant role on accelerating TP warming. Under the increasing trend of aerosol content, the fractions of absorption species should be controlled to weaken aerosol warming effect in TP.

It should be noted that the observation over Lhasa lasted for a short time in this study. To get comprehensive knowledge about aerosol impacts on TP warming and the spatial heterogeneities, it is necessary to measure multiple and long-term aerosol optical and physical parameters at more typical sites in the future. Meanwhile, vertical aerosol optical property observations based on in situ techniques are necessary to evaluate vertical aerosol effects, as remote sensing means have their limitations under extremely low aerosol content.

Data Availability Statement

The observational data is available from Wang et al. (2024). The computer program for the MRS calculation is produced by Wu (2017). The SBDART model is produced by Ricchiazzi (2017). The active fire product can be obtained from VIIRS (2021). The WRF model is available from NCAR (2022). The NCEP FNL data can be obtained from NCEP (2000). The NCEP ADP global upper air observational weather data is from NCEP (2004a), and global surface observational weather data is from NCEP (2004b).

Acknowledgments
This work was supported by the National Natural Science Foundation of China (42022051, 42305074, 42105138, 42375188), the Natural Science Foundation of Anhui Province (2108085QD181), the HFIPS Director's Fund (YZJJ2021QN02, YZJJ202101), the Second Tibetan Plateau Scientific Expedition and Research Program (2019QZKK0604), and the Youth Innovation Promotion Association CAS (Y202089). We thank Cheng Chen (Laboratoire d'Optique Atmosphérique, Université Lille) for discussion on this work.

References

Bond, T. C., Doherty, S. J., Fahey, D. W., Forster, P. M., Berntsen, T., DeAngelo, B. J., et al. (2013). Bounding the role of black carbon in the climate system: A scientific assessment. *Journal of Geophysical Research: Atmospheres*, *118*(11), 5380–5552. https://doi.org/10.1002/jgrd.50171

Che, H., Qi, B., Zhao, H., Xia, X., Eck, T. F., Goloub, P., et al. (2018). Aerosol optical properties and direct radiative forcing based on measurements from the China Aerosol Remote Sensing Network (CARSNET) in eastern China. *Atmospheric Chemistry and Physics*, *18*(1), 405–425. https://doi.org/10.5194/acp-18-405-2018

Chen, B., Chao, W. C., & Liu, X. (2002). Enhanced climatic warming in the Tibetan Plateau due to doubling CO_2: A model study. *Climate Dynamics*, *20*(4), 401–413. https://doi.org/10.1007/s00382-002-0282-4

Chen, S., Wang, W., Li, M., Mao, J., Ma, N., Liu, J., et al. (2022). The contribution of local anthropogenic emissions to air pollutants in Lhasa on the Tibetan plateau. *Journal of Geophysical Research: Atmospheres*, *127*(17), e2021JD036202. https://doi.org/10.1029/2021JD036202

Chylek, P., & Wong, J. (1995). Effect of absorbing aerosols on global radiation budget. *Geophysical Research Letters*, *22*(8), 929–931. https://doi.org/10.1029/95GL00800

Cong, Z., Kang, S., Luo, C., Li, Q., Huang, J., Gao, S., & Li, X. (2011). Trace elements and lead isotopic composition of PM10 in Lhasa, Tibet. *Atmospheric Environment*, *45*(34), 6210–6215. https://doi.org/10.1016/j.atmosenv.2011.07.060

de Leeuw, G., Sogacheva, L., Rodriguez, E., Kourtidis, K., Georgoulias, A. K., Alexandri, G., et al. (2018). Two decades of satellite observations of AOD over mainland China using ATSR-2, AATSR and MODIS/Terra: Data set evaluation and large-scale patterns. *Atmospheric Chemistry and Physics*, *18*(3), 1573–1592. https://doi.org/10.5194/acp-18-1573-2018

Devi, A., & Satheesh, S. K. (2022). Global maps of aerosol single scattering albedo using combined CERES-MODIS retrieval. *Atmospheric Chemistry and Physics*, *22*(8), 5365–5376. https://doi.org/10.5194/acp-22-5365-2022

Drinovec, L., Močnik, G., Zotter, P., Prévôt, A. S. H., Ruckstuhl, C., Coz, E., et al. (2015). The "dual-spot" aethalometer: An improved measurement of aerosol black carbon with real-time loading compensation. *Atmospheric Measurement Techniques*, *8*(5), 1965–1979. https://doi.org/10.5194/amt-8-1965-2015

Duan, A., & Xiao, Z. (2015). Does the climate warming hiatus exist over the Tibetan Plateau? *Scientific Reports*, *5*(1), 13711. https://doi.org/10.1038/srep13711

Duan, Z., Gao, Z., Xu, Q., Zhou, S., Qin, K., & Yang, Y. (2022). A benchmark dataset of diurnal- and seasonal-scale radiation, heat, and CO_2 fluxes in a typical East Asian monsoon region. *Earth System Science Data*, *14*(9), 4153–4169. https://doi.org/10.5194/essd-14-4153-2022

Dubovik, O., & King, M. D. (2000). A flexible inversion algorithm for retrieval of aerosol optical properties from Sun and sky radiance measurements. *Journal of Geophysical Research*, *105*(D16), 20673–20696. https://doi.org/10.1029/2000jd900282

Dubovik, O., Smirnov, A., Holben, B. N., King, M. D., Kaufman, Y. J., Eck, T. F., & Slutsker, I. (2000). Accuracy assessments of aerosol optical properties retrieved from Aerosol Robotic Network (AERONET) Sun and sky radiance measurements. *Journal of Geophysical Research*, *105*(D8), 9791–9806. https://doi.org/10.1029/2000JD900040

Garland, R. M., Yang, H., Schmid, O., Rose, D., Nowak, A., Achtert, P., et al. (2008). Aerosol optical properties in a rural environment near the mega-city Guangzhou, China: Implications for regional air pollution, radiative forcing and remote sensing. *Atmospheric Chemistry and Physics*, *8*(17), 5161–5186. https://doi.org/10.5194/acp-8-5161-2008

Gui, K., Che, H., Tian, L., Wang, Y., Shi, C., Yao, W., et al. (2022). Columnar optical, microphysical and radiative properties of the 2022 Hunga Tonga volcanic ash plumes. *Science Bulletin*, *67*(19), 2013–2021. https://doi.org/10.1016/j.scib.2022.08.018

Guo, D., & Wang, H. (2012). The significant climate warming in the northern Tibetan Plateau and its possible causes. *International Journal of Climatology*, *32*(12), 1775–1781. https://doi.org/10.1002/joc.2388

Han, T., Xu, W., Li, J., Freedman, A., Zhao, J., Wang, Q., et al. (2017). Aerosol optical properties measurements by a CAPS single scattering albedo monitor: Comparisons between summer and winter in Beijing, China. *Journal of Geophysical Research: Atmospheres*, *122*(4), 2513–2526. https://doi.org/10.1002/2016jd025762

Helin, A., Virkkula, A., Backman, J., Pirjola, L., Sippula, O., Aakko-Saksa, P., et al. (2021). Variation of absorption Ångström exponent in aerosols from different emission sources. *Journal of Geophysical Research: Atmospheres*, *126*(10), e2020JD034094. https://doi.org/10.1029/2020jd034094

Holben, B. N., Eck, T. F., Slutsker, I., Smirnov, A., Sinyuk, A., Schafer, J., et al. (2006). Aeronet's Version 2.0 quality assurance criteria. *Proceedings of SPIE - The International Society for Optical Engineering*, *6408*, 6408Q. https://doi.org/10.1117/12.706524

Huang, J., Zhou, X., Wu, G., Xu, X., Zhao, Q., Liu, Y., et al. (2023). Global climate impacts of land-surface and atmospheric processes over the Tibetan Plateau. *Reviews of Geophysics*, *61*(3), e2022RG000771. https://doi.org/10.1029/2022RG000771

Huang, R. J., Zhang, Y., Bozzetti, C., Ho, K. F., Cao, J. J., Han, Y., et al. (2014). High secondary aerosol contribution to particulate pollution during haze events in China. *Nature*, *514*(7521), 218–222. https://doi.org/10.1038/nature13774

Kang, L., Huang, J., Chen, S., & Wang, X. (2016). Long-term trends of dust events over Tibetan Plateau during 1961–2010. *Atmospheric Environment*, *125*, 188–198. https://doi.org/10.1016/j.atmosenv.2015.10.085

Kuang, Y., He, Y., Xu, W., Zhao, P., Cheng, Y., Zhao, G., et al. (2020). Distinct diurnal variation in organic aerosol hygroscopicity and its relationship with oxygenated organic aerosol. *Atmospheric Chemistry and Physics*, *20*(2), 865–880. https://doi.org/10.5194/acp-20-865-2020

Kuang, Y., Zhao, C., Tao, J., & Ma, N. (2015). Diurnal variations of aerosol optical properties in the North China Plain and their influences on the estimates of direct aerosol radiative effect. *Atmospheric Chemistry and Physics*, *15*(10), 5761–5772. https://doi.org/10.5194/acp-15-5761-2015

Laj, P., Bigi, A., Rose, C., Andrews, E., Lund Myhre, C., Collaud Coen, M., et al. (2020). A global analysis of climate-relevant aerosol properties retrieved from the network of Global Atmosphere Watch (GAW) near-surface observatories. *Atmospheric Measurement Techniques*, *13*(8), 4353–4392. https://doi.org/10.5194/amt-13-4353-2020

Lambe, A. T., Cappa, C. D., Massoli, P., Onasch, T. B., Forestieri, S. D., Martin, A. T., et al. (2013). Relationship between oxidation level and optical properties of secondary organic aerosol. *Environmental Science and Technology*, *47*(12), 6349–6357. https://doi.org/10.1021/es401043j

Li, C., Chen, P., Kang, S., Yan, F., Hu, Z., Qu, B., & Sillanpää, M. (2016). Concentrations and light absorption characteristics of carbonaceous aerosol in PM 2.5 and PM 10 of Lhasa city. the Tibetan Plateau. *Atmospheric Environment*, *127*, 340–346. https://doi.org/10.1016/j.atmosenv.2015.12.059

Li, J., Carlson, B. E., Yung, Y. L., Lv, D., Hansen, J., Penner, J. E., et al. (2022). Scattering and absorbing aerosols in the climate system. *Nature Reviews Earth & Environment*, *3*(6), 363–379. https://doi.org/10.1038/s43017-022-00296-7

Li, J., Liu, C., Yin, Y., & Kumar, K. R. (2016). Numerical investigation on the Ångström exponent of black carbon aerosol. *Journal of Geophysical Research: Atmospheres*, *121*(7), 3506–3518. https://doi.org/10.1002/2015jd024718

Li, L., Li, Z., Li, K., Wang, Y., Tian, Q., Su, X., et al. (2020). Aerosol direct radiative effects over China based on long-term observations within the sun–sky radiometer observation network (SONET). *Remote Sensing*, *12*(20), 3296. https://doi.org/10.3390/rs12203296

Li, X., Xiao, M., Xu, X., Zhou, J., Yang, K., Wang, Z., et al. (2020). Light absorption properties of organic aerosol from wood pyrolysis: Measurement method comparison and radiative implications. *Environmental Science and Technology*, *54*(12), 7156–7164. https://doi.org/10.1021/acs.est.0c01475

Li, Z., Guo, J., Ding, A., Liao, H., Liu, J., Sun, Y., et al. (2017). Aerosol and boundary-layer interactions and impact on air quality. *National Science Review*, *4*(6), 810–833. https://doi.org/10.1093/nsr/nwx117

Liu, J., Chang, M., Cheng, Z., Zhu, S., Ding, P., Liu, F., et al. (2021). High contribution of South Asian biomass burning to Southeastern Tibetan plateau air: New evidence from radiocarbon measurement. *Environmental Science and Technology Letters*, *8*(12), 1026–1031. https://doi.org/10.1021/acs.estlett.1c00860

Loeb, N. G., & Su, W. (2010). Direct aerosol radiative forcing uncertainty based on a radiative perturbation analysis. *Journal of Climate*, *23*(19), 5288–5293. https://doi.org/10.1175/2010jcli3543.1

Lu, F., Chen, S., Hu, Z., Han, Z., Alam, K., Luo, H., et al. (2022). Sensitivity and uncertainties assessment in radiative forcing due to aerosol optical properties in diverse locations in China. *Science of the Total Environment*, *860*, 160447. https://doi.org/10.1016/j.scitotenv.2022.160447

Masson-Delmotte, V., Zhai, P., Pirani, A., Connors, S. L., Péan, C., Berger, S., et al. (2021). Climate change 2021: The physical science basis. In *Contribution of Working Group I to the Sixth Assessment Report of the Intergovernmental Panel on Climate Change*.

McComiskey, A., Schwartz, S. E., Schmid, B., Guan, H., Lewis, E. R., Ricchiazzi, P., & Ogren, J. A. (2008). Direct aerosol forcing: Calculation from observables and sensitivities to inputs. *Journal of Geophysical Research*, *113*(D9), D09202. https://doi.org/10.1029/2007jd009170

Mu, C., Abbott, B. W., Norris, A. J., Mu, M., Fan, C., Chen, X., et al. (2020). The status and stability of permafrost carbon on the Tibetan Plateau. *Earth-Science Reviews*, *211*, 103433. https://doi.org/10.1016/j.earscirev.2020.103433

NCAR (National Center for Atmospheric Research). (2022). Weather Research and Forecasting (WRF) model v4.4 [Software]. *NCAR*. Retrieved from https://github.com/wrf-model/WRF

NCEP (National Centers for Environmental Prediction). (2000). NCEP FNL Operational model global Tropospheric Analyses, continuing from July 1999 [Dataset]. *Research Data Archive at the National Center for Atmospheric Research, Computational and Information Systems Laboratory*. https://doi.org/10.5065/D6M043C6

NCEP (National Centers for Environmental Prediction). (2004b). NCEP ADP global surface observational weather data, October 1999—Continuing [Dataset]. *Research Data Archive at the National Center for Atmospheric Research, Computational and Information Systems Laboratory*. https://doi.org/10.5065/4F4P-E398

NCEP (National Centers for Environmental Prediction). (2004a). NCEP ADP global upper air observational weather data, October 1999—Continuing [Dataset]. *Research Data Archive at the National Center for Atmospheric Research, Computational and Information Systems Laboratory*. https://doi.org/10.5065/39C5-Z211

Rahman, M. M., Wang, S., Zhao, W., Arshad, A., Zhang, W., & He, C. (2023). Comprehensive evaluation of spatial distribution and Temporal trend of NO_2, SO_2 and AOD using satellite observations over South and East Asia from 2011 to 2021. *Remote Sensing*, *15*(20), 5069. https://doi.org/10.3390/rs15205069

Ramachandran, S., Rupakheti, M., & Lawrence, M. G. (2020). Aerosol-induced atmospheric heating rate decreases over South and East Asia as a result of changing content and composition. *Scientific Reports*, *10*(1), 20091. https://doi.org/10.1038/s41598-020-76936-z

Ramanathan, V., Chung, C., Kim, D., Bettge, T., Buja, L., Kiehl, J. T., et al. (2005). Atmospheric Brown clouds: Impacts on South Asian climate and hydrological cycle. *Proceedings of the National Academy of Sciences*, *102*(15), 5326–5333. https://doi.org/10.1073/pnas.0500656102

Ran, L., Deng, Z., Wu, Y., Li, J., Bai, Z., Lu, Y., et al. (2022). Measurement report: Vertical profiling of particle size distributions over Lhasa, Tibet – Tethered balloon-based in situ measurements and source apportionment. *Atmospheric Chemistry and Physics*, *22*(9), 6217–6229. https://doi.org/10.5194/acp-22-6217-2022

Rangwala, I., Miller, J. R., & Xu, M. (2009). Warming in the Tibetan Plateau: Possible influences of the changes in surface water vapor. *Geophysical Research Letters*, *36*(6), L06703. https://doi.org/10.1029/2009gl037245

Ricchiazzi, P. (2017). SBDART: Plane-parallel radiative transfer code based on DISORT and LOWTRAN band-models [Software]. *GitHub*. https://github.com/paulricchiazzi/SBDART

Ricchiazzi, P., Yang, S., Gautier, C., & Sowle, D. (1998). Sbdart: A Research and teaching software tool for plane-parallel radiative transfer in the Earth's atmosphere. *Bulletin of the American Meteorological Society*, *79*(10), 2101–2114. https://doi.org/10.1175/1520-0477(1998)079<2101:SARATS>2.0.CO;2

Saleh, R., Robinson, E. S., Tkacik, D. S., Ahern, A. T., Liu, S., Aiken, A. C., et al. (2014). Brownness of organics in aerosols from biomass burning linked to their black carbon content. *Nature Geoscience*, *7*(9), 647–650. https://doi.org/10.1038/ngeo2220

Sandradewi, J., Prévôt, A. S. H., Szidat, S., Perron, N., Alfarra, M. R., Lanz, V. A., et al. (2008). Using aerosol light absorption measurements for the quantitative determination of wood burning and traffic emission contributions to particulate matter. *Environmental Science and Technology*, *42*(9), 3316–3323. https://doi.org/10.1021/es702253m

Su, T., Li, Z., Li, C., Li, J., Han, W., Shen, C., et al. (2020). The significant impact of aerosol vertical structure on lower atmosphere stability and its critical role in aerosol–planetary boundary layer (PBL) interactions. *Atmospheric Chemistry and Physics*, *20*(6), 3713–3724. https://doi.org/10.5194/acp-20-3713-2020

Sun, Y., Du, W., Wang, Q., Zhang, Q., Chen, C., Chen, Y., et al. (2015). Real-time characterization of aerosol particle composition above the urban canopy in Beijing: Insights into the interactions between the atmospheric boundary layer and aerosol chemistry. *Environmental Science and Technology*, *49*(19), 11340–11347. https://doi.org/10.1021/acs.est.5b02373

Tao, J. C., Zhao, C. S., Ma, N., & Liu, P. F. (2014). The impact of aerosol hygroscopic growth on the single-scattering albedo and its application on the NO_2 photolysis rate coefficient. *Atmospheric Chemistry and Physics*, *14*(22), 12055–12067. https://doi.org/10.5194/acp-14-12055-2014

Tian, P., Yu, Z., Cui, C., Huang, J., Kang, C., Shi, J., et al. (2023). Atmospheric aerosol size distribution impacts radiative effects over the Himalayas via modulating aerosol single-scattering albedo. *npj Climate and Atmospheric Science*, *6*(1), 54. https://doi.org/10.1038/s41612-023-00368-5

Titos, G., Foyo-Moreno, I., Lyamani, H., Querol, X., Alastuey, A., & Alados-Arboledas, L. (2012). Optical properties and chemical composition of aerosol particles at an urban location: An estimation of the aerosol mass scattering and absorption efficiencies. *Journal of Geophysical Research*, *117*(D4), D04206. https://doi.org/10.1029/2011jd016671

Velazquez-Garcia, A., Crumeyrolle, S., de Brito, J. F., Tison, E., Bourrianne, E., Chiapello, I., & Riffault, V. (2023). Deriving composition-dependent aerosol absorption, scattering and extinction mass efficiencies from multi-annual high time resolution observations in Northern France. *Atmospheric Environment*, *298*, 119613. https://doi.org/10.1016/j.atmosenv.2023.119613

VIIRS (Visible Infrared Imaging Radiometer Suite). (2021). NRT (Near real-time) VIIRS 375 m Active Fire product VJ114IMGTDL_NRT distributed from NASA FIRMS [Dataset]. *VIIRS*. https://doi.org/10.5067/FIRMS/VIIRS/VJ114IMGT_NRT.002

Wang, B., Bao, Q., Hoskins, B., Wu, G., & Liu, Y. (2008). Tibetan Plateau warming and precipitation changes in East Asia. *Geophysical Research Letters*, *35*(14), L14702. https://doi.org/10.1029/2008gl034330

Wang, Q., Han, Y., Ye, J., Liu, S., Pongpiachan, S., Zhang, N., et al. (2019). High contribution of secondary Brown carbon to aerosol light absorption in the Southeastern Margin of Tibetan plateau. *Geophysical Research Letters*, *46*(9), 4962–4970. https://doi.org/10.1029/2019gl082731

Wang, S., Crumeyrolle, S., Zhao, W., Xu, X., Fang, B., Derimian, Y., et al. (2021). Real-time retrieval of aerosol chemical composition using effective density and the imaginary part of complex refractive index. *Atmospheric Environment*, *245*(117959), 1–14. https://doi.org/10.1016/j.atmosenv.2020.117959

Wang, S., Zhao, W., Liu, q., Zhou, J., Crumeyrolle, S., Xu, X., et al. (2024). Aerosol data over Lhasa in 2021. V2 [Dataset]. *Science Data Bank*. https://doi.org/10.57760/sciencedb.14215

Wang, X., Heald, C. L., Sedlacek, A. J., de Sá, S. S., Martin, S. T., Alexander, M. L., et al. (2016). Deriving Brown carbon from multiwavelength absorption measurements: Method and application to AERONET and aethalometer observations. *Atmospheric Chemistry and Physics*, *16*(19), 12733–12752. https://doi.org/10.5194/acp-16-12733-2016

Wu, C. (2017). Minimum R squared method (MRS) [Software]. *Zenodo*. https://doi.org/10.5281/zenodo.832396

Wu, C., Wu, D., & Yu, J. Z. (2018). Quantifying black carbon light absorption enhancement with a novel statistical approach. *Atmospheric Chemistry and Physics*, *18*(1), 289–309. https://doi.org/10.5194/acp-18-289-2018

Xu, X., Zhao, W., Fang, B., Zhou, J., Wang, S., Zhang, W., et al. (2018). Three-wavelength cavity-enhanced albedometer for measuring wavelength-dependent optical properties and single-scattering albedo of aerosols. *Optics Express*, *26*(25), 33484–33500. https://doi.org/10.1364/OE.26.033484

Xu, X., Zhao, W., Zhang, Q., Wang, S., Fang, B., Chen, W., et al. (2016). Optical properties of atmospheric fine particles near Beijing during the HOPE-J^3A campaign. *Atmospheric Chemistry and Physics*, *16*(10), 6421–6439. https://doi.org/10.5194/acp-16-6421-2016

Yan, P., Pan, X., Tang, J., Zhou, X., Zhang, R., & Zeng, L. (2009). Hygroscopic growth of aerosol scattering coefficient: A comparative analysis between urban and suburban sites at winter in Beijing. *Particuology*, *7*(1), 52–60. https://doi.org/10.1016/j.partic.2008.11.009

You, Q., Cai, Z., Pepin, N., Chen, D., Ahrens, B., Jiang, Z., et al. (2021). Warming amplification over the Arctic Pole and third Pole: Trends, mechanisms and consequences. *Earth-Science Reviews*, *217*, 103625. https://doi.org/10.1016/j.earscirev.2021.103625

Zhang, G., Peng, L., Lian, X., Lin, Q., Bi, X., Chen, D., et al. (2019). An improved absorption Ångström exponent (AAE)-Based method for evaluating the contribution of light absorption from Brown carbon with a high-time resolution. *Aerosol and Air Quality Research*, *19*(1), 15–24. https://doi.org/10.4209/aaqr.2017.12.0566

Zhang, L., Tang, C., Huang, J., Du, T., Guan, X., Tian, P., et al. (2021). Unexpected high absorption of atmospheric aerosols over a Western Tibetan plateau site in summer. *Journal of Geophysical Research: Atmospheres*, *126*(7), e2020JD033286. https://doi.org/10.1029/2020jd033286

Zhao, G., Yu, Y., Tian, P., Li, J., Guo, S., & Zhao, C. (2020). Evaluation and correction of the ambient particle spectral light absorption measured using a filter-based Aethalometer. *Aerosol and Air Quality Research*, *20*(8), 1833–1841. https://doi.org/10.4209/aaqr.2019.10.0500

Zhao, W., Xu, X., Dong, M., Chen, W., Gu, X., Hu, C., et al. (2014). Development of a cavity-enhanced aerosol albedometer. *Atmospheric Measurement Techniques*, *7*(8), 2551–2566. https://doi.org/10.5194/amt-7-2551-2014

Zhao, W., Zhang, X., Zhai, L., Shen, X., & Xu, J. (2022). Chemical characterization and sources of submicron aerosols in Lhasa on the Qinghai-Tibet Plateau: Insights from high-resolution mass spectrometry. *Science of the Total Environment*, *815*, 152866. https://doi.org/10.1016/j.scitotenv.2021.152866

Zheng, Y., Che, H., Xia, X., Wang, Y., Wang, H., Wu, Y., et al. (2019). Five-year observation of aerosol optical properties and its radiative effects to planetary boundary layer during air pollution episodes in North China: Intercomparison of a plain site and a mountainous site in Beijing. *Science of the Total Environment*, *674*, 140–158. https://doi.org/10.1016/j.scitotenv.2019.03.418

Zhou, J., Xu, X., Zhao, W., Fang, B., Liu, Q., Cai, Y., et al. (2020). Simultaneous measurements of the relative-humidity-dependent aerosol light extinction, scattering, absorption, and single-scattering albedo with a humidified cavity-enhanced albedometer. *Atmospheric Measurement Techniques*, *13*(5), 2623–2634. https://doi.org/10.5194/amt-13-2623-2020

Zhu, C. S., Cao, J. J., Hu, T. F., Shen, Z. X., Tie, X. X., Huang, H., et al. (2017). Spectral dependence of aerosol light absorption at an urban and a remote site over the Tibetan Plateau. *Science of the Total Environment*, *590–591*, 14–21. https://doi.org/10.1016/j.scitotenv.2017.03.057

Zhu, C. S., Qu, Y., Huang, H., Chen, J., Dai, W. T., Huang, R. J., & Cao, J. J. (2021). Black carbon and secondary Brown carbon, the dominant light absorption and direct radiative forcing contributors of the atmospheric aerosols over the Tibetan plateau. *Geophysical Research Letters*, *48*(11), e2021GL092524. https://doi.org/10.1029/2021gl092524

Zhu, J., Xia, X., Che, H., Wang, J., Cong, Z., Zhao, T., et al. (2019). Spatiotemporal variation of aerosol and potential long-range transport impact over the Tibetan Plateau, China. *Atmospheric Chemistry and Physics*, *19*(23), 14637–14656. https://doi.org/10.5194/acp-19-14637-2019

References From the Supporting Information

Chen, S.-H., & Sun, W.-Y. (2002). A one-dimensional time dependent cloud model. *Journal of the Meteorological Society of Japan. Ser. II*, *80*(1), 99–118. https://doi.org/10.2151/jmsj.80.99

Grell, G. A., & Freitas, S. R. (2014). A scale and aerosol aware stochastic convective parameterization for weather and air quality modeling. *Atmospheric Chemistry and Physics*, *14*(10), 5233–5250. https://doi.org/10.5194/acp-14-5233-2014

Iacono, M. J., Delamere, J. S., Mlawer, E. J., Shephard, M. W., Clough, S. A., & Collins, W. D. (2008). Radiative forcing by long-lived greenhouse gases: Calculations with the AER radiative transfer models. *Journal of Geophysical Research*, *113*(D13). https://doi.org/10.1029/2008jd009944

Janić, Z. I. (2001). Nonsingular implementation of the Mellor-Yamada level 2.5 scheme in the NCEP Meso model. *NOAA/NWS/ NCEP OfficeNote*, *437*, 61.

Janjić, Z. I. (1994). The step-mountain eta coordinate model: Further developments of the convection, viscous sublayer, and turbulence closure schemes. *Monthly Weather Review*, *122*(5), 927–945. https://doi.org/10.1175/1520-0493(1994)122<0927:TSMECM>2.0.CO;2

Tewari, M., Chen, F., Wang, W., Dudhia, J., LeMone, M., Mitchell, K., et al. (2004). In *Implementation and verification of the unified NOAH land surface model in the WRF model (Formerly Paper Number 17.5), paper presented at Proceedings of the 20th conference on weather analysis and forecasting/16th conference on numerical weather prediction*.